

PAPER

Optical transportation of micro-particles by non-diffracting Weber beams

To cite this article: Weiwei Liu *et al* 2018 *J. Opt.* **20** 125401

View the [article online](#) for updates and enhancements.




IOP | ebooks™

Bringing you innovative digital publishing with leading voices to create your essential collection of books in STEM research.

Start exploring the [collection](#) - download the first chapter of every title for free.

Optical transportation of micro-particles by non-diffracting Weber beams

Weiwei Liu, Jie Gao¹ and Xiaodong Yang¹ 

Department of Mechanical and Aerospace Engineering, Missouri University of Science and Technology, Rolla, MO 65409, United States of America

E-mail: gaojie@mst.edu and yangxia@mst.edu

Received 11 August 2018, revised 13 October 2018

Accepted for publication 22 October 2018

Published 2 November 2018



Abstract

The optical transportation of solid polystyrene particles by the non-diffracting Weber beams is demonstrated with both forward and backward motion along the parabolic main lobes of Weber beams in three dimensions. The Weber beams are generated from the complex field modulation based on the spatial light modulator for realizing the optical transportation of micrometer polystyrene particles in an optical tweezers setup. The particle motion and velocity distribution along the main lobes of Weber beams in two different parabolic shapes are characterized and compared.

Supplementary material for this article is available [online](#)

Keywords: non-diffracting beams, optical micro-manipulation, complex field modulation

(Some figures may appear in colour only in the online journal)

1. Introduction

Optical micromanipulation has become a substantial research tool in many fields since the optical tweezer was first introduced by Ashkin [1, 2]. Traditional optical tweezers employ strongly-focused light beams to realize optical trapping of microscale objects based on the counterbalancing between scattering force and gradient force [3, 4], which can provide great insights for revealing many fundamental mechanisms in life science and material science [5, 6]. With the rapid development of computational holography, advanced structured light fields have recently been considered in optical manipulation [7]. As one unique type of the structured light, non-diffracting beams such as Airy, Bessel, Mathieu and Weber beams possess propagation-invariant transverse beam profiles [8], which can offer abundant micromanipulation operations such as rotation [9] or transportation [10] of objects. On the other hand, other complex beams with different structures like optical conveyor beams and radially self-accelerating beams, for example the optical Archimedes' screw, could also provide novel optical manipulation applications [11].

It is known that the non-diffracting Weber beams are derived from the Helmholtz equation under parabolic coordinates, which own the novel parabolic landscapes in the transverse dimension [12, 13]. Due to the phase gradient in the beam, complex structured beams carrying orbital angular momentum usually are able to drive colloidal particles along special trajectories in three-dimensional (3D) space [14–17]. Typically, the focused helical Bessel beam can rotate micro-particles in a ring [14, 15]. It has also been demonstrated that the transportation trajectories of micro-particles can even be designed in various 3D curves by employing the polymorphic non-diffracting beams [8, 16, 17]. The Weber beam is one kind of novel non-diffracting beams with the orbital angular momentum distributed in transverse parabolic profile, which provides a new transportation landscape for micro-particles [12, 18]. Actually, the adjustable Weber beams with different parabolic profiles can be more flexible in transporting micro-particles as the force functions acting on particles can potentially be tuned, while their applications in optical micromanipulation has rarely been studied.

In this paper, we present the optical transportation of solid polystyrene particles along the main lobes of the non-diffracting Weber beams with different parabolic shapes. The Weber beams are generated from the complex field modulation based

¹ Authors to whom any correspondence should be addressed.

on the spatial light modulator (SLM) in the optical tweezer setup. It is shown that there exists an array of in-line vortices in the phase profile of the Weber beam, and the beam energy flow presents an interesting parabolic twisting behavior for transporting micro-particles along different parabolic tracks. In the experiment, the solid particle size is larger than the laser wavelength and the particles are driven by the Weber beams in 3D motion. The motion and velocity of particles are recorded and analyzed along the beam parabolic main lobe in the transverse dimension, in order to demonstrate the special transportation functionality of the Weber beams for micro-particles under the joint action of scattering force and gradient force. Our work presents a special situation for particle motion along the Weber beam, which may further promote the non-diffracting beams for optical micro-manipulation applications involved in many research fields.

2. Weber beam and its generation in optical tweezers

The non-diffracting beams usually convey the same intensity and energy flow distributions in the transverse dimension during beam propagation, which can provide uniform optical force functions for particles located at different propagation depths in optical micromanipulation [19]. The non-diffracting Weber beam is first derived from the Helmholtz equation in parabolic coordinates [12, 13]. For certain transverse and longitudinal wave vector components k_{\perp} and k_z , the solution for the non-diffracting Weber beam can be expressed in terms of a reduced Whittaker integral [20]:

$$\Psi(\mathbf{r}, t) = e^{-i\omega t} e^{ik_z z} \int_{-\pi}^{\pi} e^{ik_{\perp}(x \cos \varphi + y \sin \varphi)} f(\varphi) d\varphi, \quad (1)$$

where $f(\varphi)$ is the angular spectrum of field $\Psi(\mathbf{r}, t)$ defined on a ring of radius k_{\perp} in frequency space. The wave vector components k_{\perp} and k_z satisfy the relation of $k^2 = k_z^2 + k_{\perp}^2$, and k is the wave number. The time dependence $e^{-i\omega t}$ is considered in equation (1). It can be seen that the resulting optical field intensity $I = |\Psi(\mathbf{r}, t)|^2$ is independent on the propagation coordinate z . Different kinds of non-diffracting beams such as Bessel, Mathieu and Weber beams are determined by the special angular spectrum fields $f(\varphi)$, and for the continuous Weber beam $f(\varphi)$ is taken as follows [20]

$$f(\varphi) = (\pi |\sin \varphi|)^{-1/2} \exp(ia \cdot \ln |\tan \varphi/2|) \text{ for } \varphi \in (0, \pi) \quad (2)$$

$$f(\varphi) = 0 \text{ for } \varphi \in [-\pi, 0], \quad (3)$$

where a is the separation constant which can adjust the parabolic shape of Weber beam in the transverse dimension.

In order to reveal the particle manipulation mechanism with the Weber beam along the parabolic beam lobe, the transverse intensity and energy flow distributions are calculated for the Weber beams with a of 1.5 and 4, as shown in figures 1(a) and (b). The energy flow is calculated as the transverse component of the Poynting vector by $S = \frac{i}{4\eta_0 k_{\perp}} [\Psi \nabla \Psi^* - \Psi^* \nabla \Psi]$ [21], where $\eta_0 = \sqrt{\mu_0/\epsilon_0}$ is the impedance of free space. The Weber beams consist of

well-defined parabolic fringes with a parabolic dark region. It can be observed that the parameter a can modulate the bending of the beam parabolic shape, and the larger a gives the less beam bending for the parabolic profile. It is also seen that the energy flow follows the same direction along the parabolic fringes for the Weber beam, which indicates that the single-direction scattering force function will be applied on micro-particles along the transverse parabolic fringes, which is similar to the Bessel and Mathieu beams in optical micromanipulation [18]. Concretely, the reason for energy flow in one direction is the existence of a large amount of in-line vortices with unitary charge rotating in the same direction in the phase profile [12], as shown in figures 1(c) and (d), resulting in the overall transverse energy flow along the parabolic intensity crest of the beam main lobe.

Here the Weber beam transportation experiment for large polystyrene particles with the size of $5 \mu\text{m}$ is conducted. The particle motion velocity and direction in the complex beam are usually determined by the radiation force function based on the special structure of light field. However, in the current experiment, the gradient force function applied on particles from the focusing structure at the beam transverse center cannot be neglected, because the particle size is far larger than the laser wavelength [22]. Thus, the particle transportation experiment will provide the great insight into the combined effects of the radiation force and gradient force functions from the structured Weber beams. In order to implement the particle transportation, a typical holographic optical tweezers setup based on a microscope is constructed to generate the non-diffracting Weber beam inside the sample chamber, which enables complex field modulation employing the off-axis phase hologram [4]. The experimental setup is shown as figure 2(a) with the laser wavelength of 532 nm. The laser beam is first expanded by convex lens L1 and L2 and then is incident on the SLM with a small angle. The convex lens L3 and L4 constitute the typical $4f$ system with a pinhole in the Fourier plane which can select the first-order component for the Weber beam from the encoded phase hologram [4]. The modulated phase hologram is designed based on the overlay of transverse light beam plus one deflection grating with the phase hologram of $H = |\Psi| \{ [ky \sin(\theta) + \arg(\Psi)] \bmod 2\pi \}$ [4, 18], where k is the wave number, y is the coordinate on the SLM, and θ is the deflection angle of grating. The calculated phase hologram on the SLM for generating the Weber beam is shown in figure 2(b). The modulated beam is then focused by convex lens L5 ($f = 250 \text{ mm}$) and coupled into the sample chamber by the microscope objective lens ($\text{NA} = 1.3, 100\times$). For exploring the particle motion driven by the non-diffracting Weber beam, a CCD camera is used to record the particle motion in bright field and also the chamber thickness is large enough to allow the particle motion in 3D. Figure 2(c) displays the measured transverse intensity profiles of the generated Weber beams with $a = 1.5$ and 4 inside the sample chamber, which are in good consistence with the simulation results in figure 1.

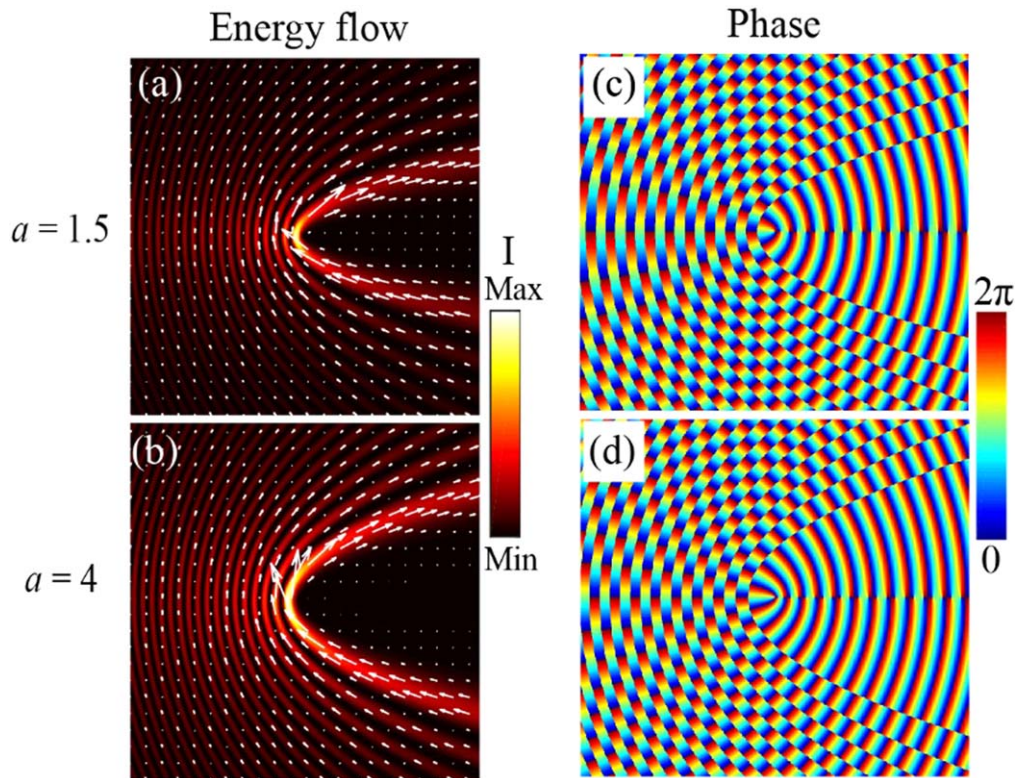


Figure 1. Transverse intensity (color map), energy flow (white arrows) and phase (color map) distributions for the non-diffracting Weber beams with different separation constants of $a = 1.5$ and 4 .

3. Particle transportation by Weber beam

The realization of particle transportation in optical micro-manipulation has important potential in many biomedical and optofluidic applications. Figure 3 presents the results of optical transportation for micrometer polystyrene spheres by the non-diffracting Weber beams, with the time-sequenced images taken from the recorded video clips to show the dynamic process of particle motion. The fixed laser power of 20 mW before entering the microscope objective lens is applied for both Weber beams. Polystyrene particles with the diameter of $5 \mu\text{m}$ are suspended in the water solution inside the sample chamber. It is observed that the main lobe of the Weber beam can transport particles stably in the parabolic trajectory due to the gradient force perpendicular to the beam trajectory, just as the Bessel-vortex beam does [18]. Since the particle also move along the beam propagation direction due to the scattering force function in the z direction, in figure 3 it can be seen that the images of particles are out of focus during the transportation within the limited distance along the beam main lobe. Thus, in the measurement, single particle is transported section by section along the parabolic beam track to map the overall manipulation ability of the Weber beam. The parabolic coordinate along the main lobe of Weber beam is defined as s . The particle motion directions along the lower ($s < 0 \mu\text{m}$) branch in figures 3(a)(a') and (d)(d') and the upper ($s > 8 \mu\text{m}$) branch in figures 3(c)(c') and (f)(f') of the main lobe are consistent with the energy flow direction in the transverse dimension. However, particles at the middle-upper ($0 < s < 8 \mu\text{m}$) region

of the main lobe will move in the opposite direction toward the central region in figures 3(b) and (e) and also have a transverse balance position close to the central region as shown in figures 3(b') and (e'), which is caused by the stronger gradient force applied on the particles than the scattering force in this region. It can also be found that by modifying the parameter a , the optical transportation of micro-particles will be constrained in the different parabolic beam tracks.

On the other hand, as particles moving along the parabolic main lobe of Weber beam in the transverse direction, transportation of particles in the axial direction (beam propagation direction) is also involved due to the axial radiation pressure force of the non-diffracting Weber beam. Such axial propulsion of particles is verified by the observed defocused particle imaging as shown in figure 4. The $t = 0$ is the time when the particle is just loaded in the main lobe of Weber beam. As displayed in figures 4(a)–(d), the transverse position of the particle in the middle (around $s = 0 \mu\text{m}$) region of beam's main lobe keeps invariant, but the particle moves stably along the axial direction. This indicates that there exists one needle-like transportation channel in the non-diffracting Weber beam along the axial direction, which is a unique feature that can greatly benefit the applications of particle transportation in a straight channel. It is noted that such needle-like transportation channel cannot be realized by other non-diffracting beams such as Bessel beams or Mathieu beams. Furthermore, figures 4(e)–(h) show that the Weber beam can drive particles moving along the main lobe in both the transverse and axial directions simultaneously, which

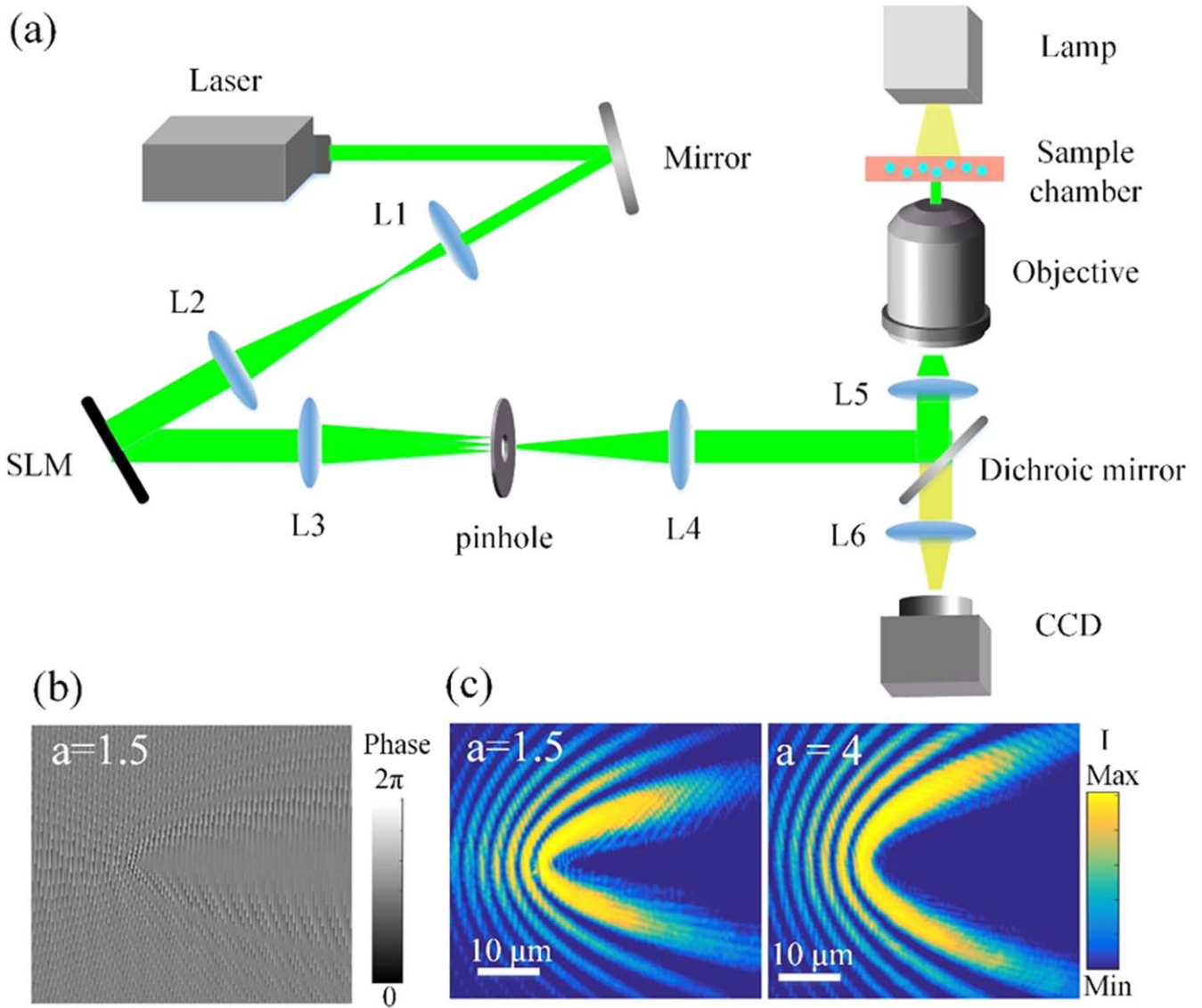


Figure 2. (a) Experimental optical tweezers setup to implement the particle transportation with the Weber beam. (b) Encoded phase profile to generate the Weber beam with complex field modulation method. (c) Experimental transverse intensity profiles for the Weber beams with $a = 1.5$ and 4 .

indicates the 3D particle transportation capability of non-diffracting Weber beam in the parabolic coordinates. Thus, the non-diffracting Weber beams will enable further important applications in 3D particle sorting and optical propulsion.

Actually, the transportation velocity of the particles does not keep invariant in the transverse dimension of the Weber beams. Figure 5 gives the average value and standard error of the particle's transverse transportation velocity along the parabolic fringes of the Weber beams with different separation constants $a = 1.5$ and 4 . There are five group data in each data point in figure 5 and the direction of the parabolic coordinate s is consistent with the energy flow direction. Firstly, it can be seen that for the region of $s < 0 \mu\text{m}$ along the beam main lobe, the transportation velocity of particle as the particle approaches the center region of beam is larger than the velocity as the particle leaves away from the center for both Weber beams. This is because the direction of gradient force is towards the beams center with higher intensity,

so that the gradient force will accelerate the particle when it approaches the center. On the contrary, for the region of $s > 8 \mu\text{m}$ the gradient force will decelerate the particle when it moves away from the center region. For the region of $0 < s < 8 \mu\text{m}$, the particle velocity is defined as negative as the particle travels towards the beam center in the opposite direction, where the gradient force is larger than the scattering force. Then we can see that the particle velocity in the region $0 < s < 8 \mu\text{m}$ of the Weber beam with $a = 1.5$ is larger than that of the Weber beam with $a = 4$. This phenomenon is caused by the stronger gradient force for the Weber beam with narrower parabolic shape ($a = 1.5$) than that for the Weber beam with wider parabolic shape ($a = 4$). Actually, from figure 1 we can see that the intensity distribution around the center region of the Weber beam is similar to the focused Gaussian beam distribution. The center region of the Weber beam with smaller a is more focused, thus leading to the stronger gradient force, compared with the Weber beam with

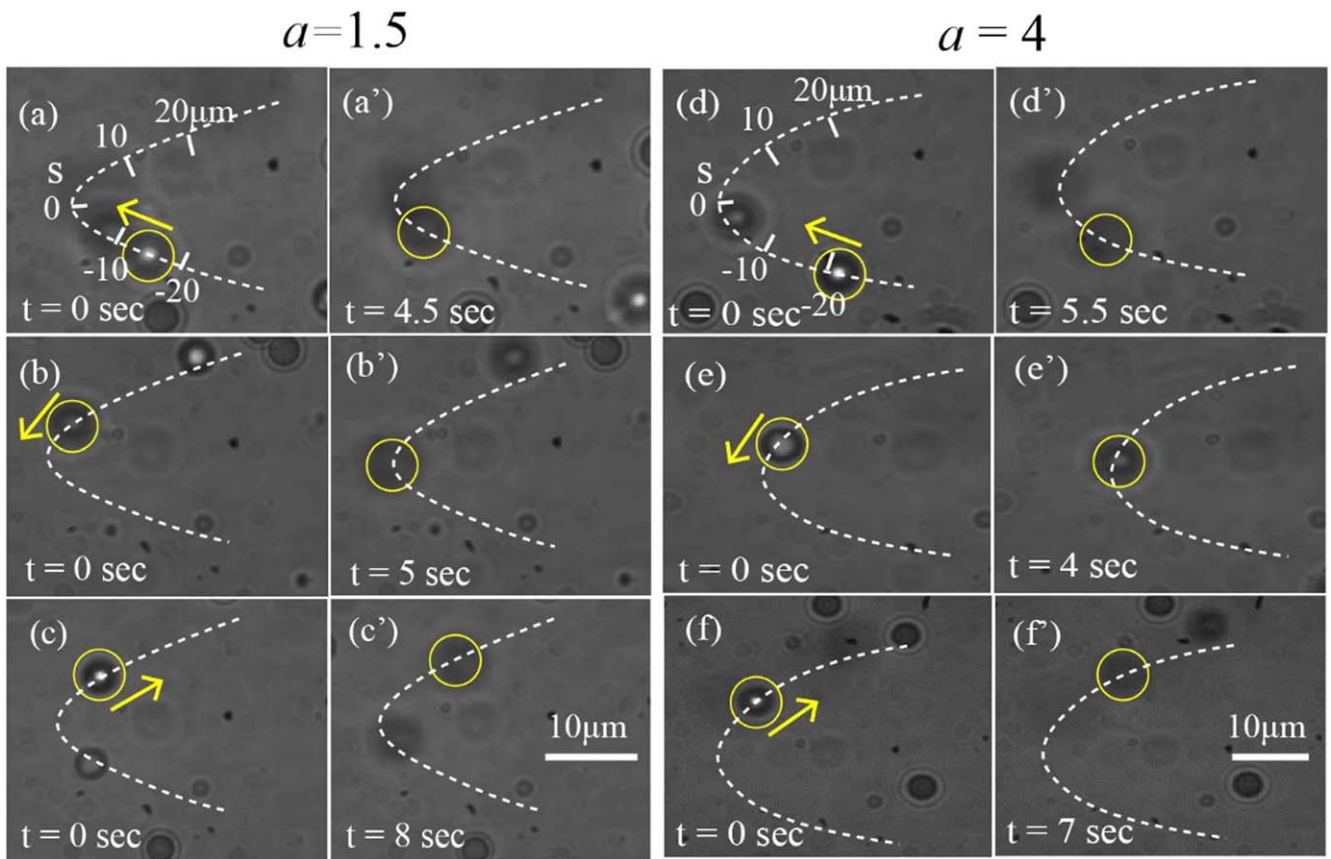


Figure 3. Optical transportation of micro-particles along the main-lobe of non-diffracting Weber beams with separation constants $a = 1.5$ and 4. (a)(a'), (b)(b') and (c)(c') The time-sequenced images to show single particle motion in lower ($s < 0 \mu\text{m}$), middle-upper ($0 < s < 8 \mu\text{m}$) and upper ($s > 8 \mu\text{m}$) branches of the main-lobe for the Weber beam with $a = 1.5$ (media 1). (d)(d'), (e)(e') and (f)(f') Results for particle motion in the Weber beam with $a = 4$ (media 2). The parabolic dashed lines and yellow circles indicate the position of the main lobe and the particle outline, respectively. The arrow in the figure shows the transverse motion direction of the particles along the main lobe of Weber beam. The $t = 0$ is the moment when the particle is just loaded in the beam's main lobe.

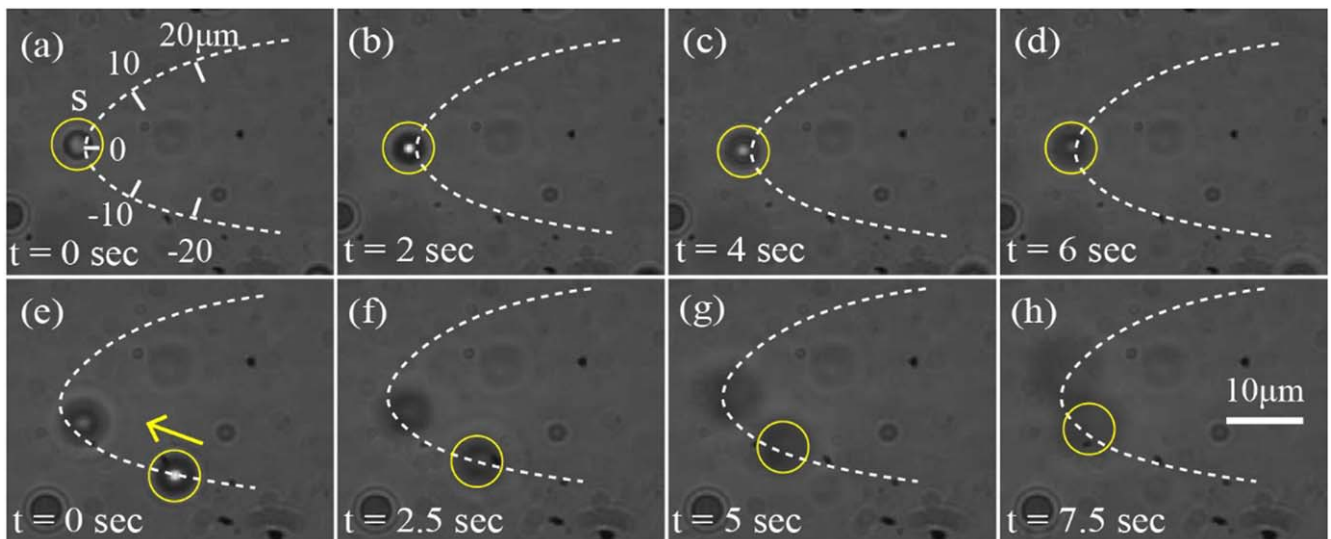


Figure 4. Particle transportation in axial direction in the main lobe of Weber beam with $a = 4$, with the time-sequenced images showing the axial motion of single particle in the middle (around $s = 0 \mu\text{m}$) region (a)–(d) (media 3) and in the lower ($s < 0 \mu\text{m}$) branch of the beam's main lobe (e)–(h) (media 2). The parabolic dashed line and yellow circle indicate the position of the main lobe and the particle outline, respectively. The arrow in (e) shows the transverse motion direction of the particle along the main lobe of Weber beam.

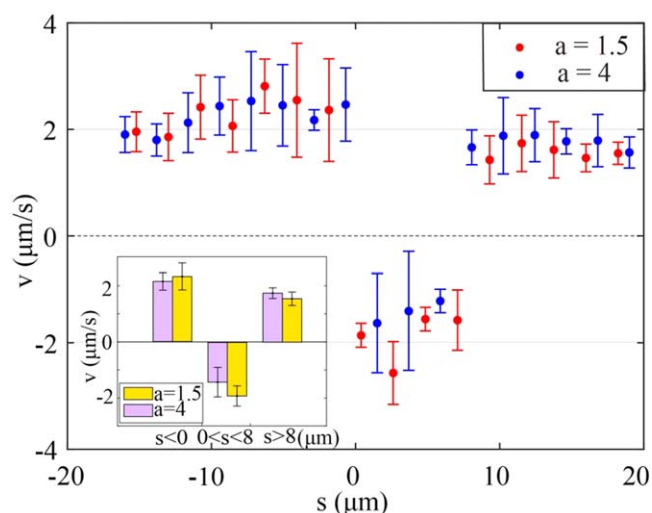


Figure 5. Transportation velocity of the particles along the parabolic main lobe of the Weber beams with different separation constants $a = 1.5$ (red) and 4 (blue). The inset shows the average velocity for the particle in the three regions of $s < 0 \mu\text{m}$, $0 < s < 8 \mu\text{m}$, and $s > 8 \mu\text{m}$.

larger a . This theory about the gradient force variation in the focused Gaussian beam has been well explained [22]. For further demonstrating the gradient force function for the motion of large particles in the Weber beams, the inset in figure 5 shows the average velocity of polystyrene particle in the above three regions of $s < 0 \mu\text{m}$, $0 < s < 8 \mu\text{m}$, $s > 8 \mu\text{m}$. It is indicated that the stronger gradient force achieved in the more focused Weber beam with $a = 1.5$ will accelerate the particle more with higher average velocities of $2.3 \mu\text{m s}^{-1}$ and $-1.9 \mu\text{m s}^{-1}$ in the beam's regions of $s < 0 \mu\text{m}$, $0 < s < 8 \mu\text{m}$, compared to the average velocities of $2.1 \mu\text{m s}^{-1}$ and $-1.5 \mu\text{m s}^{-1}$ in these two regions of Weber beam with $a = 4$. On the other hand, the relative stronger gradient force will also obstruct the particle transportation further in the beam's region of $s > 8 \mu\text{m}$, leading to the average velocity in this region of Weber beam with $a = 1.5$ lower than that in the Weber beam with $a = 4$, with the average velocity of $1.54 \mu\text{m s}^{-1}$ and $1.74 \mu\text{m s}^{-1}$, respectively. Through the above analysis, we can see that the Weber beam with wider parabolic shape (larger a) can transport particles more smoothly.

4. Conclusion

The optical transportation of solid polystyrene particles by the non-diffracting Weber beams with different parabolic shapes has been demonstrated. The unique energy flow of the Weber beam existed in parabolic distribution is analyzed, which reflects the scattering force acting on the particles. The non-diffracting Weber beams are generated by employing the complex field modulation based on the SLM. Our results show that the structured Weber beams can transport micro-scale particles along the parabolic beam main lobe in the same direction as that of the energy flow. Meanwhile, it is also

demonstrated that the particles can move in the opposite direction towards the beam center when the particles are in the middle-upper ($0 < s < 8 \mu\text{m}$) region of beam main lobe. Through the analysis of the transportation velocity in the parabolic trajectory for the two Weber beams with different separation constants, it is shown that the Weber beam with wider parabolic shape can transport particles more smoothly. In the future, by dynamically addressing the holograms encoded on the SLM, advanced reconfigurable optical manipulation for particles can be demonstrated. For example, the dynamic process can be designed to transport different sizes of biological objects to different locations by switching the Weber beams with different parabolic parameters. Our results will not only advance the development of optical micromanipulation with complex structured beams, but also greatly benefit many photonics applications of controllable non-diffracting beams in various research fields.

Acknowledgments

The authors acknowledge support from the NASA Innovative Advanced Concepts (NIAC) (NNX16AL26G) and the Office of Naval Research (N00014-16-1-2408).

ORCID iDs

Xiaodong Yang  <https://orcid.org/0000-0001-9031-3155>

References

- [1] Ashkin A, Dziedzic J M, Bjorkholm J E and Chu S 1986 Observation of a single-beam gradient force optical trap for dielectric particles *Opt. Lett.* **11** 288
- [2] Ashkin A, Dziedzic J M and Yamane T 1987 Optical trapping and manipulation of single cells using infrared laser beams *Nature* **330** 769
- [3] Ashkin A 1970 Acceleration and trapping of particles by radiation pressure *Phys. Rev. Lett.* **24** 156
- [4] Gong L, Liu W, Zhao Q, Ren Y, Qiu X, Zhong M and Li Y 2016 Controllable light capsules employing modified Bessel–Gauss beams *Sci. Rep.* **6** 29001
- [5] Block S M, Goldstein L S and Schnapp B J 1990 Bead movement by single kinesin molecules studied with optical tweezers *Nature* **348** 348
- [6] Wang X, Dai Y, Zhang Y, Min C and Yuan X 2018 Plasmonic manipulation of targeted metallic particles by polarization-sensitive metalens *ACS Photonics* **5** 2945–50
- [7] Wördemann M 2012 *Structured Light Fields: Applications in Optical Trapping, Manipulation, and Organisation* (Berlin: Springer) (<https://doi.org/10.1007/978-3-642-29323-8>)
- [8] Levy U, Derevyanko S and Silberberg Y 2016 Light modes of free space *Prog. Opt.* **61** 237–81
- [9] Volke-Sepulveda K, Garcés-Chávez V, Chávez-Cerda S, Arit J and Dholakia K 2002 Orbital angular momentum of a high-order Bessel light beam *J. Opt. B: Quantum Semiclass. Opt.* **4** 82
- [10] Davis J A, Mintry M J, Bandres M A and Cottrell D M 2008 Observation of accelerating parabolic beams *Opt. Express* **16** 12866–71

- [11] Hadad B, Froim S, Nagar H, Admon T, Eliezer Y and Roichman Y 2018 Particle trapping and conveying using an optical Archimedes screw *Optica* **5** 551–6
- [12] López-Mariscal C, Bandres M A, Gutiérrez-Vega J C and Chávez-Cerda S 2005 Observation of parabolic nondiffracting optical fields *Opt. Express* **13** 2364–9
- [13] Bandres M A, Gutiérrez-Vega J C and Chávez-Cerda S 2004 Parabolic nondiffracting optical wave fields *Opt. Lett.* **29** 44–6
- [14] Roichman Y, Sun B, Roichman Y, Amato-Grill J and Grier D G 2008 Optical forces arising from phase gradients *Phys. Rev. Lett.* **100** 013602
- [15] Shanblatt E R and Grier D G 2011 Extended and knotted optical traps in three dimensions *Opt. Express* **19** 5833–8
- [16] Rodrigo J A and Alieva T 2015 Freestyle 3D laser traps: tools for studying light-driven particle dynamics and beyond *Optica* **2** 812–5
- [17] Rodrigo J A and Alieva T 2016 Polymorphic beams and nature inspired circuits for optical current *Sci. Rep.* **6** 35341
- [18] Ortiz-Ambriz A, Gutiérrez-Vega J C and Petrov D 2014 Manipulation of dielectric particles with nondiffracting parabolic beams *J. Opt. Soc. Am. A* **31** 2759–62
- [19] Zhao J, Chremmos I D, Song D, Christodoulides D N, Efremidis N K and Chen Z 2015 Curved singular beams for three-dimensional particle manipulation *Sci. Rep.* **5** 12086
- [20] Diebel F, Rose P, Boguslawski M and Denz C 2016 Observation of spatially oscillating solitons in photonic lattices *New J. Phy.* **18** 053038
- [21] Broky J, Siviloglou G A, Dogariu A and Christodoulides D N 2008 Self-healing properties of optical Airy beams *Opt. Express* **16** 12880–91
- [22] Ashkin A 1992 Forces of a single-beam gradient laser trap on a dielectric sphere in the ray optics regime *Biophys. J.* **61** 569–82